Journal of Systems Engineering and Electronics
Vol. 33, No. 2, April 2022, pp.426 – 437

A trajectory shaping guidance law with field-of-view angle constraint and terminal limits

FU Shengnan[1], ZHOU Guanqun[2,*], and XIA Qunli[3]

1. School of Mechatronical Engineering, Beijing Institute of Technology, Beijing 100081, China;
2. Beijing Aerospace Technology Institute, Beijing 100074, China;
3. School of Aerospace Engineering, Beijing Institute of Technology, Beijing 100081, China

Abstract: In this paper, a trajectory shaping guidance law, which considers constraints of field-of-view (FOV) angle, impact angle, and terminal lateral acceleration, is proposed for a constant speed missile against a stationary target. First, to decouple constraints of the FOV angle and the terminal lateral acceleration, the third-order polynomial with respect to the line-of-sight (LOS) angle is introduced. Based on an analysis of the relationship between the looking angle and the guidance coefficient, the boundary of the coefficient that satisfies the FOV constraint is obtained. The terminal guidance law coefficient is used to guarantee the convergence of the terminal conditions. Furthermore, the proposed law can be implemented under bearings-only information, as the guidance command does not involve the relative range and the LOS angle rate. Finally, numerical simulations are performed based on a kinematic vehicle model to verify the effectiveness of the guidance law. Overall, the work offers an easily implementable guidance law with closed-form guidance gains, which is suitable for engineering applications.

Keywords: shaping guidance law, field-of-view (FOV) constraint, impact angle constraint, terminal lateral acceleration constraint.

DOI: 10.23919/JSEE.2022.000043

1. Introduction

For the terminal guidance of a vehicle, in many cases, the guidance law is required to intercept the target precisely with the desired impact angle to maximize the warhead effectiveness [1−3]. To realize a large impact angle, the guidance law may cause the trajectory to be highly curved, and increase the looking angle. If the looking angle exceeds the field-of-view (FOV) angle constraint, it may result in a mission failure [4−6]. Thus, when designing an impact angle control, it is very important to consider the seeker's FOV angle constraint. Besides, it is also necessary to ensure the convergence of the terminal lateral acceleration, so that the trajectory can be easily realized in practice.

The impact angle constraint is imposed on the terminal flight path angle to improve warhead effectiveness and lethality. For example, the penetration weapon needs to attack the target with a nearly vertical impact angle. Kim [7] studied the impact angle constraint firstly. They transformed a linearized engagement geometry problem into a linear quadratic optimization problem and introduced a suboptimal guidance law for reentry vehicles to intercept a non-maneuverable target. Ryoo [8] proposed practical and precise time-to-go calculation methods by approximating the missile trajectory as a third-order polynomial of time-to-go. The designed guidance law is the resultant command which is a linear combination of a step and a ramp acceleration response of the missile. An extension of that work was presented in [9] with a polynomial of order and the engagement geometry problem was transformed into a linear-quadratic optimal control problem, where the energy cost is weighted by a power of time-to-go. Kim et al. [10] derived a backstep guidance law which required the information of the line-of-sight (LOS) angle, impact angle, and estimated time-to-go. Kumar et al. [11] proposed a sliding-mode-control-based guidance law to intercept stationary, constant-velocity, and maneuvering targets at the desired impact angle. Oza et al. [12] proposed a suboptimal guidance law through the model predictive static programming technique. The guidance law is three-dimensional which can satisfy terminal impact angle constraints in both azimuth and elevation directions. In these studies, the estimation of time-to-go is important, which requires the implementation of precise time-to-go calculation methods.

Proportional navigation (PN) [13] and its variants are widely used because of its simple structure and strong ro-

Manuscript received November 23, 2020.
*Corresponding author.
This work was supported by the Defense Science and Technology Key Laboratory Fund of Luoyang Electro-Optical Equipment Institute, Aviation Industry Corporation of China (6142504200108).

bustness. A three-dimensional adaptive PN is used by Lu et al. [14] to satisfy the impact angle constraint, which is applied to design the terminal guidance for hypersonic vehicles. Ratnoo et al. [15] proposed a two-stage guidance law based on the PN guidance to intercept a stationary target with the desired impact angle. In the first stage a lower navigation gain is used to achieve the desired direction to switch to the second stage, and in the second stage a higher navigation gain is used to achieve the terminal constraint. An extension of that work was presented in [16] for non-maneuvering target interception with the desired impact angle. Erer et al. [17] proposed a guidance law with a bias term to the pure PN guidance command. Therein, a two-stage guidance scheme was designed to control the impact angle. Zhang et al. [18] designed a biased PN law for the large impact angle control problem, which satisfies constraints of impact time and impact angle. Zhang et al. [19] proposed a biased PN guidance law with impact time and impact angle constraints. To eliminate the time-to-go error, a feedback control with adjustable coefficients is introduced to control the impact time and impact angle simultaneously. In these studies, the impact angle constraint and other constraints are considered based on the PN guidance law. However, the guarantees on the FOV constraint are not discussed.

Considering the engineering application, the FOV constraint of the seeker also needs to be introduced. Kim et al. [20] presented the PN guidance law with switch supplementary time-varying bias terms considering the impact angle constraint and FOV angle constraint. Erer et al. [21] proposed the biased pure PN and the unbiased PN guidance laws, and designed the gain guidance schemes. Furthermore, the lateral acceleration constraint was introduced [22]. For three typical cases, different guidance laws were designed. Park et al. [23] proposed an energy optimal guidance law. A three-stage guidance scheme was designed to realize different constraints in different stages. A range-to-go weighted performance index was introduced [24] using a similar guidance law. To achieve all impact angles with the FOV angle constraint, a two-stage PN guidance law was presented by Ratnoo [25]. The impact angle for the FOV angle constraint can be obtained in an analytical form. The above multi-constraint guidance laws were designed for different stages. However, the switching of different guidance laws may cause problems in engineering applications.

The adaptive multi-constraint guidance law becomes very popular in recent years. Jeon et al. [26] proposed an impact-time-control guidance law. The closed-form time-varying navigation gain can be obtained from the missile-to-target range and angle information. Based on the sliding mode control method, Kim et al. [24] proposed a new guidance law. Liu et al. [27] proposed a multi-constraint guidance law for stationary and non-maneuvering moving targets. The core idea is to transform into the limit of the relative speed perpendicular to the LOS angle between the missile and the target. Sharma et al. [28] proposed a two-gain feedback guidance law based on the bearings-only information. A feasible implementable region is deduced in impact angle-maximum looking angle design space. The guidance law has a simple form, and the guidance gain is easy to calculate. However, in some extreme cases, the terminal lateral acceleration is too large, which is difficult to realize in practice.

In this study, we propose an impact angle control guidance law that restricts the looking angle within the FOV angle constraint. The main contribution of the paper is that the proposed method introduces a third-order polynomial with respect to the LOS angle, and satisfies the convergence requirement of the terminal lateral acceleration, FOV angle constraint, and impact angle constraint. The guidance gain can be adjusted adaptively depending on the desired looking angle. Based on the analysis of the characteristics of the third-order polynomial, we transform the FOV angle constraint into the range of the coefficient for the looking angle, and give the analytical boundary of the looking angle to satisfy the FOV constraint. By the design of the coefficient for the looking angle and the terminal guidance law coefficient respectively, the proposed guidance law can satisfy multiple constraints simultaneously. Compared with the traditional optimal guidance law [29], the proposed guidance law does not need the information on the time-to-go, and the FOV angle constraint is added and satisfied.

The paper is organized as follows. In Section 2, the problem statement is given. In Section 3, the third-order polynomial shaping guidance law is designed. The characteristics of the looking angle are analyzed. In Section 4, the feasible guidance gains are obtained according to the boundary of the looking angle. In Section 5, the simulation results are presented to validate the performance of the proposed guidance laws. Finally, the conclusions are given in Section 6.

2. Problem statement

Considering a two-dimensional surface-to-surface engagement scenario as shown in Fig. 1, where M represents the center of mass of the missile and T represents the center of mass of the target. Assuming that the angle of attack is small, the lead angle is approximately equal to the looking angle. That is, the seeker's FOV angle can be controlled by adjusting the looking angle. For a stationary target, assuming that the missile velocity is constant, non-

linear engagement kinematics in a polar coordinate system can be expressed as

$$\begin{cases} \dfrac{\mathrm{d}R}{\mathrm{d}t} = -V\cos\sigma \\ \dfrac{\mathrm{d}\sigma}{\mathrm{d}t} = \dfrac{\mathrm{d}\gamma}{\mathrm{d}t} - \dfrac{\mathrm{d}\lambda}{\mathrm{d}t} = \dfrac{a}{V} + \dfrac{V\sin\sigma}{R} \\ \dfrac{\mathrm{d}\gamma}{\mathrm{d}t} = \dfrac{a}{V} \end{cases} \tag{1}$$

where R is the missile-target relative range, V is the velocity of the missile, a is the lateral acceleration, γ is the flight path angle, λ is the LOS angle, σ is the looking angle, which is defined as the angle between the LOS and the velocity vector, and t represents the time as an independent variable.

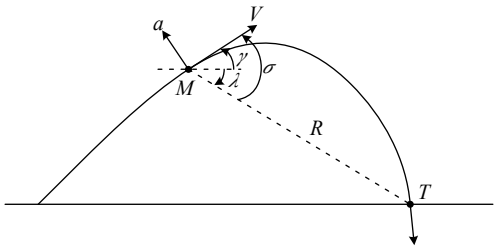

Fig. 1 Engagement scenario

For a surface-to-surface engagement scenario, the initial LOS angle is zero, and other initial conditions are given by

$$\begin{cases} R(t_0) = R_0 \\ \sigma(t_0) = \gamma(t_0) = \sigma_0 \\ \lambda(t_0) = 0 \end{cases} \tag{2}$$

where the subscript 0 represents the initial states.

Similarly, considering the constraint of the desired impact angle γ_f, the terminal conditions are given by

$$\begin{cases} R(t_f) = 0 \\ \sigma(t_f) = 0 \\ \gamma(t_f) = \lambda(t_f) = \gamma_f \end{cases} \tag{3}$$

where the subscript f represents the terminal states.

Moreover, the terminal lateral acceleration needs to realize the convergence for engineering applications, given by

$$a(t_f) = 0. \tag{4}$$

Assume that the maximum seeker's FOV angle is denoted as $\sigma_{\max}$. the looking angle during the whole flight should be limited by

$$|\sigma| \leqslant \sigma_{\max}. \tag{5}$$

Equations (1)−(5) describe the terminal guidance problem in a two-dimensional plane considering the impact angle constraint and the FOV angle constraint of the seeker. For most terminal guidance problems with a stationary target, the looking angle is usually within the range $(-\pi/2, \pi/2)$.

3. Guidance design

Since the missile-target relative range R is monotonically decreasing, some shaping guidance laws are designed as polynomial functions with independent variables R or t:

$$\sigma(R) = k_N R^N + k_{N-1}R^{N-1} + \cdots + k_2 R^2 + k_1 R + k_0 \tag{6}$$

where k_N, k_{N-1},$\cdots$, k_0 are polynomial coefficients, decided by initial conditions, terminal conditions, and other constraints. Using (6), the deduced guidance law often includes time-to-go t_{go}, which needs precise calculation methods in consideration of a curved trajectory. In order to reduce the complexity of the guidance law, the independent variable λ is introduced. In a surface-to-surface engagement scenario, we can notice that the LOS angle λ will monotonously change. Thus, the one-to-one mapping between the state and the missile-target relative range R can be transformed into the mapping between the state and the LOS angle λ. Using the form of (6), we design a polynomial function as

$$\sigma(\lambda) = k_N\lambda^N + k_{N-1}\lambda^{N-1} + \cdots + k_2\lambda^2 + k_1\lambda + k_0. \tag{7}$$

Differentiating the looking angle σ with respect to the flight time, $\dfrac{\mathrm{d}\sigma}{\mathrm{d}t}$ can be transferred into $\dfrac{\mathrm{d}\sigma(\lambda)}{\mathrm{d}\lambda}\cdot\dfrac{\mathrm{d}\lambda}{\mathrm{d}t}$. Thus, we can get the shaping guidance law:

$$\begin{aligned} a = V\frac{\mathrm{d}\gamma(t)}{\mathrm{d}t} = V\left(\frac{\mathrm{d}\sigma(t)}{\mathrm{d}t} + \frac{\mathrm{d}\lambda(t)}{\mathrm{d}t}\right) = \\ \left[\frac{\mathrm{d}\sigma(\lambda)}{\mathrm{d}\lambda} + 1\right]V\frac{\mathrm{d}\lambda}{\mathrm{d}t} = M_\lambda V\frac{\mathrm{d}\lambda}{\mathrm{d}t} \end{aligned} \tag{8}$$

where M_λ is an adaptive guidance law coefficient.

Equation (8) is similar to the PN guidance law. If the terminal adaptive guidance law coefficient is larger than 2, the guidance law can realize the convergence of the terminal lateral acceleration.

The second-order polynomial shaping guidance law is derived from [28]. In some cases, the terminal lateral acceleration cannot converge to zero. Based on the analysis of the second-order polynomial shaping guidance law, we can notice that the maximum looking angle is related to the terminal adaptive guidance law coefficient. We may not be able to limit the maximum looking angle within the FOV angle constraint and the terminal adaptive guidance law coefficient to greater than 2 simultaneously. That is, there may be contradictions that the FOV angle constraint and the terminal lateral acceleration constraint

cannot be satisfied at the same time.

To solve this problem, a third-order polynomial shaping guidance law is designed in this section. Using adjustable coefficients c_1 and M_f, we can control the maximum looking angle and the terminal adaptive guidance law coefficient individually, to realize the FOV angle and terminal lateral acceleration constraints separately.

3.1 Guidance law

If $N = 3$, (7) can be rewritten as

$$\sigma(\lambda) = k_3\lambda^3 + k_2\lambda^2 + k_1\lambda + k_0 \tag{9}$$

where k_0, k_1, k_2 and k_3 are polynomial coefficients.

For convenience, the terminal guidance law coefficient $M(q_f)$ is recorded as M_f . That is, the terminal condition needs to be satisfied with

$$\left.\frac{\mathrm{d}\sigma}{\mathrm{d}\lambda}\right|_{\lambda=\lambda_f} = M_f - 1. \tag{10}$$

where $M_f - 1$ determines the terminal looking angle rate, which can be designed as a constant to satisfy the terminal constraint.

Based on the constraint in (10), we design the following form of the looking angle rate as

$$\frac{\mathrm{d}\sigma}{\mathrm{d}\lambda} = c_1(\lambda-\lambda_f)^2 + c_2(\lambda-\lambda_f) + (M_f - 1) \tag{11}$$

where $c_1 (c_1 \neq 0)$ and c_2 are coefficients for the looking angle, which are designed to satisfy the FOV angle constraint of the seeker.

The integral of (11) is obtained as

$$\sigma(\lambda) = \frac{c_1(\lambda-\lambda_f)^3}{3} + \frac{c_2(\lambda-\lambda_f)^2}{2} + (M_f - 1)(\lambda-\lambda_f) + c_3 \tag{12}$$

where c_3 is another coefficient for the looking angle.

Using (2) and (3), a relationship between coefficients for the looking angle can be deduced by rearranging (12) as

$$\begin{cases} c_3 = 0 \\ c_2 = \dfrac{2c_1}{3}\lambda_f + \dfrac{2(M_f - 1 + \sigma_0/\lambda_f)}{\lambda_f} \end{cases}. \tag{13}$$

Using (13), (11) and (12) can be rearranged as

$$\frac{\mathrm{d}\sigma}{\mathrm{d}\lambda} = c_1(\lambda-\lambda_f)\left(\lambda - \frac{1}{3}\lambda_f\right) + \frac{2(M_f - 1 + \sigma_0/\lambda_f)}{\lambda_f}\cdot (\lambda-\lambda_f) + (M_f - 1), \tag{14}$$

$$\sigma(\lambda) = \frac{c_1(\lambda-\lambda_f)^2\lambda}{3} + \frac{(M_f 1 + \sigma_0/\lambda_f)(\lambda-\lambda_f)\lambda}{\lambda_f} - \frac{\sigma_0}{\lambda_f}(\lambda-\lambda_f). \tag{15}$$

Using (8) and (14), the closed-loop guidance law can be obtained as

$$a = \left[c_1(\lambda-\lambda_f)\left(\lambda - \frac{1}{3}\lambda_f\right) + \frac{2(M_f - 1 + \sigma_0/\lambda_f)}{\lambda_f}(\lambda-\lambda_f) + M_f\right]V\frac{\mathrm{d}\lambda}{\mathrm{d}t}. \tag{16}$$

To analyze the FOV angle, (15) can be divided into two parts as follows:

$$\begin{cases} \sigma_c(\lambda) = \dfrac{c_1(\lambda-\lambda_f)^2\lambda}{3} \\ \sigma_M(\lambda) = \dfrac{(M_f - 1 + \sigma_0/\lambda_f)(\lambda-\lambda_f)\lambda}{\lambda_f} - \dfrac{\sigma_0}{\lambda_f}(\lambda-\lambda_f) \end{cases}. \tag{17}$$

We can notice that $\sigma_c(\lambda)$ is related to the coefficient c_1 and σ_M is related to the terminal guidance law coefficient. The next section will analyze the characteristics of $\sigma_c(\lambda)$ and σ_M separately corresponding to the path characteristics and the terminal characteristics.

3.2 Path characteristics

To keep the analysis simple and understandable, nondimensionalization should be applied. Dimensionless states are defined as $\bar{\lambda} = -\lambda/\lambda_f$, $\bar{\sigma} = -\sigma/\lambda_f$, $\bar{\sigma}_c = -\sigma_c/\lambda_f$ and $\bar{c}_1 = -c_1\lambda_f{}^2$. Using (17), we can get

$$\bar{\sigma}_c(\bar{\lambda}) = \frac{\bar{c}_1}{3}\left(\bar{\lambda}+1\right)^2\bar{\lambda}. \tag{18}$$

Differentiating (18) with respect to the LOS angle $\bar{\lambda}$ leads to

$$\frac{\mathrm{d}\bar{\sigma}_c}{\mathrm{d}\bar{\lambda}} = \frac{\bar{c}_1}{3}\left(\bar{\lambda}+1\right)\left(3\bar{\lambda}+1\right). \tag{19}$$

On imposing $\mathrm{d}\bar{\sigma}_c/\mathrm{d}\bar{\lambda} = 0$, the dimensionless LOS angle at the maximum dimensionless looking angle $\bar{\sigma}_{c\max}$ can be derived as

$$\bar{\lambda}_{\bar{\sigma}_{c\max}} = -\frac{1}{3}. \tag{20}$$

Using (18) and (20), the maximum looking angle can be deduced as

$$\bar{\sigma}_{c\max} = -\frac{4}{81}\bar{c}_1. \tag{21}$$

Fig. 2 shows the variation of $\bar{\sigma}_c$ for different $\bar{c}_1$ with respect to $\bar{\lambda}$, and the maximum values are marked with points. The coefficient c_1 for the looking angle affects the

maximum looking angle $\bar{\sigma}_{c\max}$ and the LOS angle $\bar{\lambda}_{\bar{\sigma}_{c\max}}$ is constant as $-1/3$.

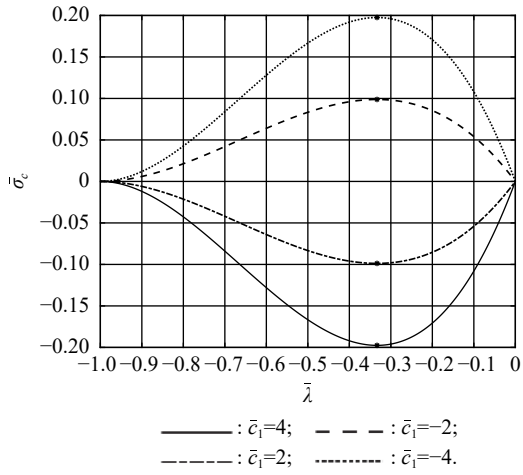

Fig. 2 $\bar{\sigma}_t$ **for different** $\bar{c}_1$ **with respect to** $\bar{\lambda}$

3.3 Terminal characteristics

The dimensionless state is defined as $\bar{\sigma}_M = -\sigma_M/\lambda_f$. Using (17), we can get

$$\bar{\sigma}_M(\bar{\lambda}) = -(M_f - 1 + \sigma_0/\lambda_f)(\bar{\lambda}+1)\bar{\lambda} - \sigma_0/\lambda_f(\bar{\lambda}+1). \tag{22}$$

Differentiating (22) with respect to the LOS angle $\bar{\lambda}$ leads to

$$\frac{\mathrm{d}\bar{\sigma}_M}{\mathrm{d}\bar{\lambda}} = -2(M_f - 1 + \sigma_0/\lambda_f)\bar{\lambda} - (M_f - 1 + 2\sigma_0/\lambda_f). \tag{23}$$

On imposing $\mathrm{d}\bar{\sigma}_M/\mathrm{d}\bar{\lambda} = 0$, we can notice that, if $\sigma_0/\lambda_f \geqslant (M_f - 1)/2$, $\bar{\sigma}_M$ is monotonically increasing and the maximum looking angle is $\bar{\sigma}_{M\max} = -\sigma_0/\lambda_f$ at $\bar{\lambda} = 0$. If $\sigma_0/\lambda_f < (M_f - 1)/2$, the dimensionless LOS angle at the maximum dimensionless looking angle $\bar{\sigma}_{M\max}$ can be derived as

$$\bar{\lambda}_{\bar{\sigma}_{M\max}} = -\frac{1}{2} - \frac{\sigma_0/\lambda_f}{2(M_f - 1 + \sigma_0/\lambda_f)}. \tag{24}$$

Using (22) and (24), the maximum looking angle $\bar{\sigma}_{M\max}$ corresponding to the terminal characteristics can be deduced as

$$\bar{\sigma}_{M\max} = \frac{(M_f - 1)^2}{4(M_f - 1 + \sigma_0/\lambda_f)}. \tag{25}$$

Fig. 3 shows the variations $\bar{\sigma}_M$ for different σ_0/λ_f with respect to $\bar{\lambda}$ and $M_f = 3$, and maximum values are marked with points. The value of σ_0/λ_f affects the maximum looking angle $E_{M\max}$ and the LOS angle $\bar{\lambda}_{\bar{\sigma}_{M\max}}$ at the maximum dimensionless looking angle.

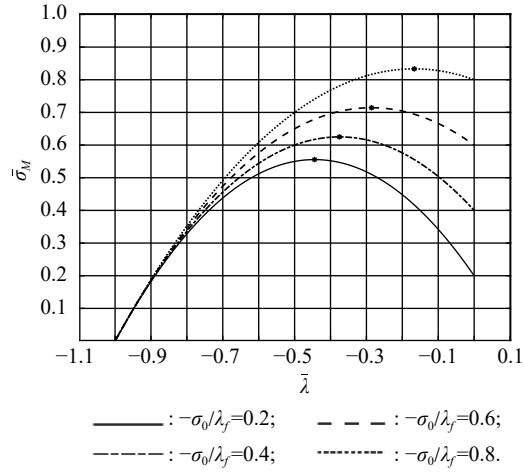

Fig. 3 ε_M **for different** σ_0/λ_f **with respect to** $\bar{\lambda}$

3.4 Dimensionless looking angle

From Subsection 3.2 and Subsection 3.3, we can notice that the main function of the term $\bar{\sigma}_c$ is to control the looking maximum angle without affecting the initial and terminal conditions. The main function of the term $\bar{\sigma}_M$ is to satisfy initial and terminal conditions. Once the terminal guidance law coefficient M_f is determined, the maximum looking angle should only be controlled by $\bar{c}_1$.

Using (18) and (22), we can get the dimensionless looking angle:

$$\bar{\sigma}(\bar{\lambda}) = (\bar{\lambda}+1)\left[\frac{\bar{c}_1}{3}(\bar{\lambda}+1)\bar{\lambda} - (M_f - 1 + \sigma_0/\lambda_f)\bar{\lambda} - \sigma_0/\lambda_f\right]. \tag{26}$$

Differentiating (26) with respect to the LOS angle $\bar{\lambda}$ leads to

$$\frac{\mathrm{d}\bar{\sigma}}{\mathrm{d}\bar{\lambda}} = \bar{c}\bar{\lambda}^2 + \left[\frac{4\bar{c}_1}{3} - 2(M_f - 1 + \sigma_0/\lambda_f)\right]\bar{\lambda} + \left[\frac{\bar{c}}{3} - (M_f - 1 + 2\sigma_0/\lambda_f)\right]. \tag{27}$$

Using (27), we can get another form of the dimensionless looking angle as

$$\bar{\sigma}(\bar{\lambda}) = \frac{(\bar{\lambda}+1)}{2}\frac{\mathrm{d}\bar{\sigma}}{\mathrm{d}\bar{\lambda}} - \frac{\bar{c}_1(\bar{\lambda}+1)^3}{6} + \frac{(M_f - 1)(\bar{\lambda}+1)}{2}. \tag{28}$$

To get the maximum dimensionless looking angle, we suppose that in $\bar{\lambda} \in (-1, 0)$, we can get $\dfrac{\mathrm{d}\bar{\sigma}(\bar{\lambda}_{\bar{\sigma}_{\max}})}{\mathrm{d}\bar{\lambda}} = 0$. Using (28), we can get the maximum looking angle deduced as

$$\bar{\sigma}_{\max} = -\frac{\bar{c}_1(\bar{\lambda}_{\bar{\sigma}_{\max}}+1)^3}{6} + \frac{(M_f - 1)(\bar{\lambda}_{\bar{\sigma}_{\max}}+1)}{2}. \tag{29}$$

4. Feasible guidance gains

The looking angle $\bar{\sigma}$ can be controlled by the coefficient $\bar{c}_1$ of the looking angle to realize the FOV angle constraint. To achieve a feasible guidance gain, we need to focus on the boundary of $\bar{\varepsilon}$. Fig. 2 shows that the lower boundary of the coefficient $\bar{c}_1$ corresponds to the maximum value of the looking angle. Conversely, the upper boundary of the coefficient $\bar{c}_1$ corresponds to the maximum value of the looking angle. Thus, the range of the looking angle can be controlled by the coefficient $\bar{c}_1$.

4.1 The lower boundary

Denote the lower boundary of $\bar{c}_1$ as $\bar{c}_{1L}$. If $\sigma_0/\lambda_f = -(M_f-1)/4$, $\bar{\lambda}_{\bar{\sigma}_{c\max}} = \bar{\lambda}_{\bar{\sigma}_{M\max}} = \bar{\lambda}_{\bar{\sigma}_{\max}} = -1/3$, using (21) and (25), we can get the maximum looking angle:

$$\bar{\sigma}_{\max} = -\frac{4}{81}\bar{c}_{1L} + \frac{4}{3}\frac{\sigma_0}{\lambda_f}. \tag{30}$$

Thus, we can get the lower boundary $\bar{c}_{1L}$ as

$$\bar{c}_{1L} = -\frac{81}{4}\bar{\sigma}_{\max} + 27\frac{\sigma_0}{\lambda_f}. \tag{31}$$

If $\sigma_0/\lambda_f \neq -(M_f-1)/4$ and $\bar{\lambda}_{\bar{\sigma}_{\max}} \neq -1/3$, according to (27), we can get $\dfrac{\mathrm{d}\bar{\sigma}}{\mathrm{d}\bar{\lambda}} = 0$ for the maximum looking angle. Thus, we can get the lower boundary $\bar{c}_{1L}$ as

$$\bar{c}_{1L} = \frac{2(M_f - 1 + \sigma_0/\lambda_f)\left(\bar{\lambda}_{\bar{\sigma}_{\max}} + 1\right) - (M_f - 1)}{\left(\bar{\lambda}_{\bar{\sigma}_{\max}} + 1\right)\left(\bar{\lambda}_{\bar{\sigma}_{\max}} + \dfrac{1}{3}\right)}. \tag{32}$$

Proposition For $\bar{\lambda}_{\bar{\sigma}_{\max}} \in [-1, 0]$, there must be a $\bar{\lambda}_{\bar{\sigma}_{\max}}$ for the lower boundary.

Proof Using (29) and (32), we can get the maximum looking angle for $\bar{\lambda}_{\bar{\sigma}_{\max}} \neq -1/3$ as

$$\bar{\sigma}_{\max} = \frac{-(M_f - 1 + \sigma_0/\lambda_f)\left(\bar{\lambda}_{\bar{\sigma}_{\max}} + 1\right)^3}{\left(3\bar{\lambda}_{\bar{\sigma}_{\max}} + 1\right)} + \frac{2(M_f - 1)\left(\bar{\lambda}_{\bar{\sigma}_{\max}} + 1\right)^2 - (M_f - 1)\left(\bar{\lambda}_{\bar{\sigma}_{\max}} + 1\right)}{\left(3\bar{\lambda}_{\bar{\sigma}_{\max}} + 1\right)}. \tag{33}$$

Equation (33) can be transformed into the following form:

$$f(\bar{\lambda}_{\bar{\sigma}_{\max}}) = (M_f - 1 - \sigma_0/\lambda_f)\left(\bar{\lambda}_{\bar{\sigma}_{\max}} + 1\right)^3 - 2(M_f - 1)\left(\bar{\lambda}_{\bar{\sigma}_{\max}} + 1\right)^2 + (M_f - 1 + 3\bar{\sigma}_{\max})\left(\bar{\lambda}_{\bar{\sigma}_{\max}} + 1\right) - 2\bar{\sigma}_{\max}. \tag{34}$$

Fig. 4 shows the variation of $f(\bar{\lambda}_{\bar{\sigma}_{\max}})$ for different σ_0/λ_f with $M_f = 3$ and $\bar{\sigma}_{\max} = 2\bar{\sigma}_0$. Since $f(-1) = -2\bar{\sigma}_{\max} < 0$ and $f(0) = \bar{\sigma}_{\max} + \sigma_0/\lambda_f \geqslant 0$, we can obtain $\bar{\lambda}_{\bar{\sigma}_{\max}}$ in the range $[-1, 0]$. □

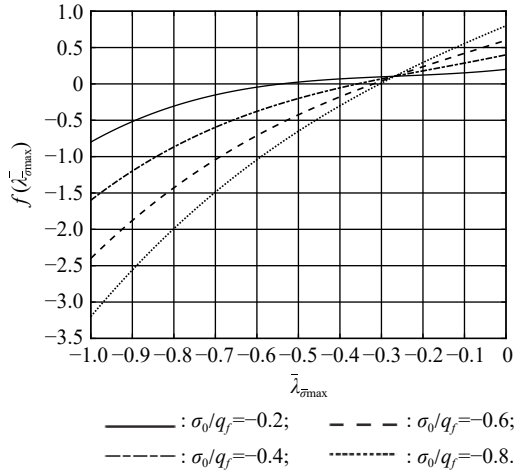

Fig. 4 $f\left(\bar{\lambda}_{a_{\min}}\right)$ **for different** σ_0/λ_f **with respect to** $\bar{\lambda}_{\bar{\sigma}\max}$

4.2 The upper boundary

For a surface-to-surface engagement scenario, $\bar{\sigma}(\bar{\lambda})$ needs to keep the symbol unchanged during the whole trajectory. Considering an extreme case, there are both maximum looking angle $\sigma_{\max}$ and minimum looking angle $\bar{\sigma}_{\min} = 0$ during a trajectory. The process to obtain the minimum looking angle $\bar{\sigma}_{\min}$ and maximum value $\bar{\sigma}_{\max}$ are similar. Thus, using (34), we can get

$$(M_f - 1 + \sigma_0/\lambda_f)\left(\bar{\lambda}_{\bar{\sigma}_{\min}} + 1\right)^2 - 2(M_f - 1)\left(\bar{\lambda}_{\bar{\sigma}_{\min}} + 1\right) + (M_f - 1) = 0. \tag{35}$$

Using (35), the dimensionless LOS angle at the minimum dimensionless looking angle $\bar{\sigma}_{\min}$ can be derived as

$$\bar{\lambda}_{\bar{\sigma}_{\min}} = -\frac{\sqrt{\sigma_0/\lambda_f}}{\sqrt{\sigma_0/\lambda_f} + \sqrt{M_f - 1}}. \tag{36}$$

Denote the upper boundary of $\bar{c}_1$ as $\bar{c}_{1U}$. Using (33) and (36), the upper boundary $\bar{c}_{1U}$ can be derived as

$$\bar{c}_{1U} = 3\left(\sqrt{\sigma_0/\lambda_f} + \sqrt{M_f - 1}\right)\cdot\left[(M_f - 1)\sqrt{M_f - 1} - \sqrt{\sigma_0/\lambda_f (M_f - 1)}\left(2\sqrt{\sigma_0/\lambda_f} + \sqrt{M_f - 1}\right)\right]\cdot \frac{1}{\left(M_f - 1 - 2\sqrt{\sigma_0/\lambda_f (M_f - 1)}\right)}. \tag{37}$$

In conclusion, the range of the dimensionless coefficient $\bar{c}_1$ for the looking angle satisfying the FOV angle constraint of the seeker can be concluded as

$$\bar{c}_{1L} \leqslant \bar{c}_1 \leqslant \bar{c}_{1U}. \tag{38}$$

Convert (38) to a dimensional form by $c_{1L} = \bar{c}_{1L}/\lambda_f^2$ and $c_{1U} = \bar{c}_{1U}/\lambda_f^2$, shown as

$$c_{1L} \leqslant c_1 \leqslant c_{1U}. \tag{39}$$

To verify the effectiveness of the designed boundary, we design a typical case with $M_f = 3$, $\bar{\sigma}_{\max} = 2\bar{\sigma}_0$, and $\sigma_0/\lambda_f = -0.4$. Fig. 5 shows that if $\omega_1 = \varphi_{1L}$, the looking angle reaches the maximum value, and if $c_1 = c_{1U}$, the looking angle reaches the maximum value and the minimum value. Thus, if the coefficient satisfies $c_{1L} \leqslant c_1 \leqslant c_{1U}$, the FOV angle constraint, initial and terminal conditions can be satisfied.

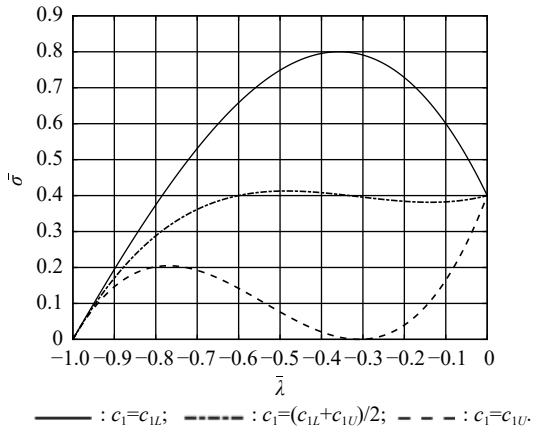

Fig. 5 σ for different c_1 with respect to $\bar{\lambda}$

5. Simulation results

The third-order shaping guidance law of (16) is used for simulation. A typical case is designed as the velocity $V = 1\,000$ m/s, the initial missile-target relative range $R_0 = 50$ km, the initial LOS angle $\lambda_0 = 0°$, and the initial looking angle $\sigma_0 = 15°$. The desired impact angle is $\gamma_f = -80°$. All simulations are terminated for a miss distance $R < 1 \times 10^{-3}$ m. To determine the terminal guidance law coefficient M_f, we need to study the influence of M_f first.

5.1 Influence of the terminal guidance law coefficient

We can notice that the designed shaping guidance law is similar to the PN guidance law. Thus, the terminal guidance law coefficient is designed as $M_f \geqslant 2$ to realize the convergence of the terminal lateral acceleration. To analyze the influence of the terminal guidance law coefficient, we design some typical cases. The FOV angle constraint is $\sigma_{\max} = 30°$. Different terminal guidance law coefficients are verified as M_f =2, 2.5, 3, 3.5. The coefficient ω_1 for the looking angle is designed by the lower boundary to realize the maximum value. Using (24), we can get the LOS angle $\bar{\lambda}_{\bar{\sigma}_{\max}}$ at the maximum looking angle. Using (39), we can get coefficients c_1 for different terminal guidance law coefficients as

$$c_1 = \begin{cases} -0.710\,4, & M_f = 2 \\ 0.599\,4, & M_f = 2.5 \\ 2.188\,1, & M_f = 3 \\ 4.189\,5, & M_f = 3.5 \end{cases}.$$

The simulation results are shown in Fig. 6–Fig. 11. The missile trajectories are plotted in Fig. 6. The successful interceptions with the desired impact angle are shown in Fig. 7 and Fig. 8. Fig. 9 shows the variation in the looking angle with respect to time. A higher value of the terminal guidance law coefficient M_f corresponds to a lower maximum height of the trajectory and a lower time to adjust terminal angles. That is, the time that the looking angle reaches the FOV angle constraint is later.

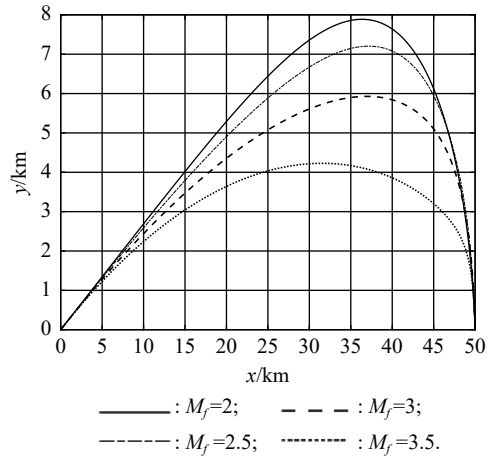

Fig. 6 Missile trajectories

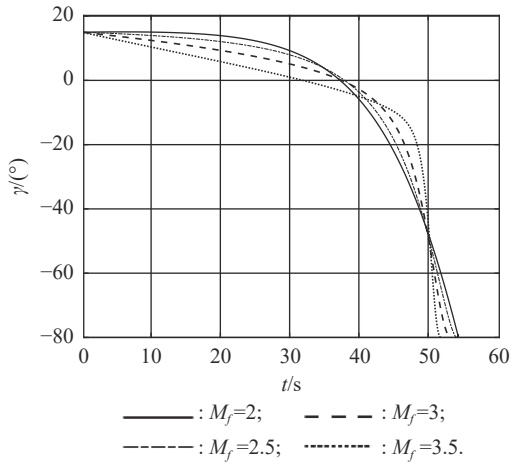

Fig. 7 Flight path angle profiles

The variations in the lateral acceleration and adaptive guidance law coefficients are shown in Fig. 10 and Fig. 11. If the terminal guidance law coefficient M_f is designed too large, the maximum lateral acceleration will be a large value. Conversely, if M_f is designed too small, the terminal lateral acceleration may not achieve the convergence.

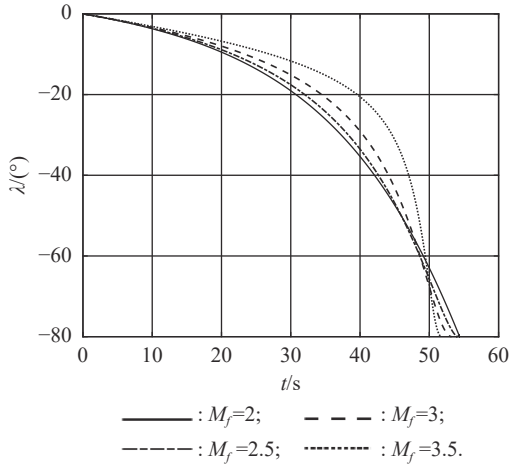

Fig. 8 LOS angle profiles

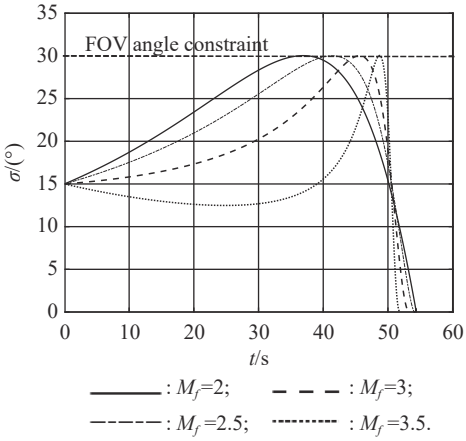

Fig. 9 Looking angle profiles

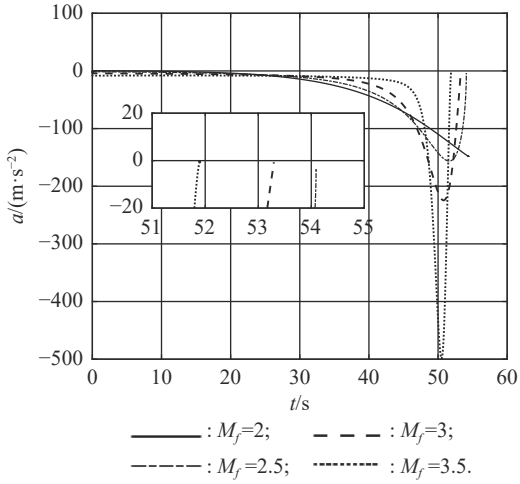

Fig. 10 Lateral acceleration profiles

Considering both the terminal convergence requirement and the maximum lateral acceleration constraint, we design the terminal guidance law coefficient as $M_f = 3$ in this paper. If the dynamic lag and disturbance factors will be considered in future studies, the terminal guidance law coefficient should be increased properly.

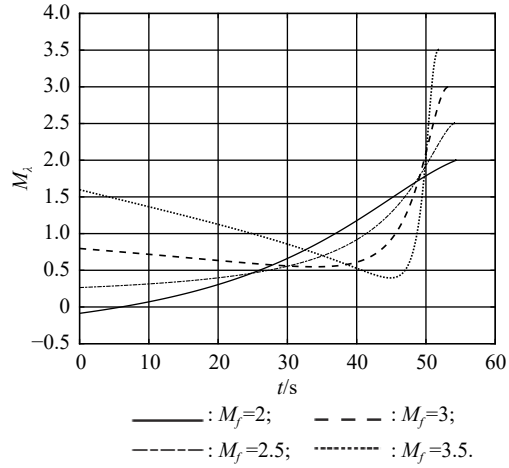

Fig. 11 Adaptive guidance law coefficient profiles

5.2 Comparison studies

The optimal guidance law(OGL)[29] is the most widely used guidance law in engineering for the impact angle constraint. The form of OGL is shown as follows:

$$a = 2(n+2)V\frac{\mathrm{d}\lambda}{\mathrm{d}t} + (n+1)(n+2)\frac{V}{t_{\mathrm{go}}}(\lambda - \lambda_f) \tag{40}$$

where n is the guidance law coefficient, t_{go} is the time-to-go, decided by R/V. To realize the convergence of the terminal lateral acceleration, the guidance law coefficient needs to satisfy $n > 0$. In this paper, we design the guidance law coefficient for OGL as $n = 0.5$.

The form of the second-order polynomial guidance law in [28] is shown as follows:

$$a = \left[k_2(2\lambda - \lambda_f) - \frac{\sigma_0}{\lambda_f} + 1\right]V\frac{\mathrm{d}\lambda}{\mathrm{d}t} \tag{41}$$

where k_2 is the guidance law coefficient. The derivation process for the range of the guidance law coefficient is similar to that of the third-order guidance law, which will not be discussed in this paper. And the guidance law coefficient k_2 is set to be −0.581 9.

In this section, the simulation is carried out for shaping guidance laws ($N = 2, N = 3$) and OGL to verify the effectiveness of the proposed guidance law. To compare the performance of different guidance laws, we design a typical case. The terminal guidance law coefficient is $M_f = 3$.

Since OGL cannot satisfy the FOV angle constraint, it is necessary to ensure that the maximum value of the looking angle to be consistent for different guidance laws. According to the pre-verified simulation for OGL, the maximum looking angle is about 65.04°. Thus, for shaping guidance laws, the FOV angle constraint is set to $\sigma_{\max} = 65.04°$.

For $N = 3$, the coefficient for the looking angle c_1 can

be decided by the proposed boundaries. Using (32) and (37), we can get boundaries as $c_{1L} = -2.837\ 3$ and $c_{1U} = 5.250\ 8$. For $N = 2$, we design an extreme case to prove that the second-order shaping guidance law may not be able to realize the convergence of the terminal lateral acceleration.

Fig. 12–Fig. 18 show the simulation results of the comparison between the second-order shaping guidance law, the third-order shaping guidance law, and OGL. In Fig. 12, the trajectories for $N = 3(c_1 = -2.837\ 3)$ and OGL correspond to the maximum looking angle, and trajectories for $N = 2$ and $N = 3(c_1 = 5.250\ 8)$ correspond to the upper boundary of guidance coefficients to realize the minimum looking angle. Fig. 13 and Fig. 14 show that the flight path angle and LOS angle change rapidly at the end for the second-order and third-order shaping guidance laws. Fig. 15 shows that for the lower boundary of the third-order shaping guidance law, the looking angle can reach the FOV angle constraint. For the upper boundary, the looking angle also changes rapidly at the end.

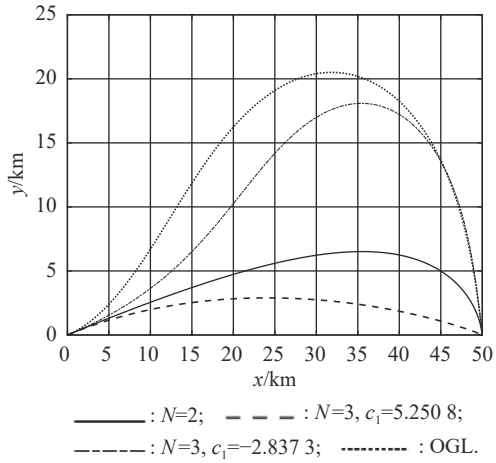

Fig. 12 Missile trajectories

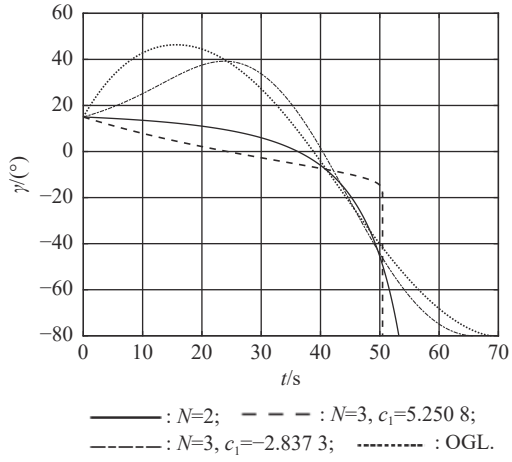

Fig. 13 Flight path angle profiles with respect to time

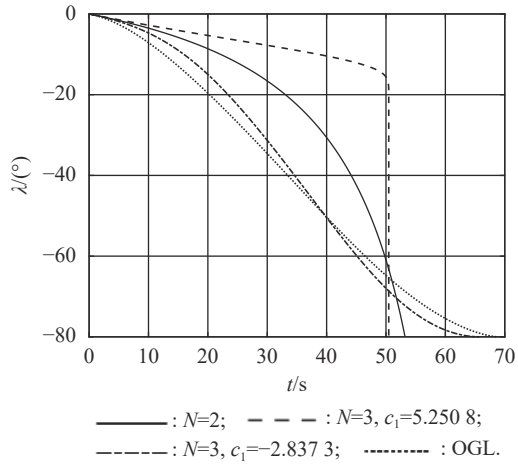

Fig. 14 LOS angle profiles with respect to time

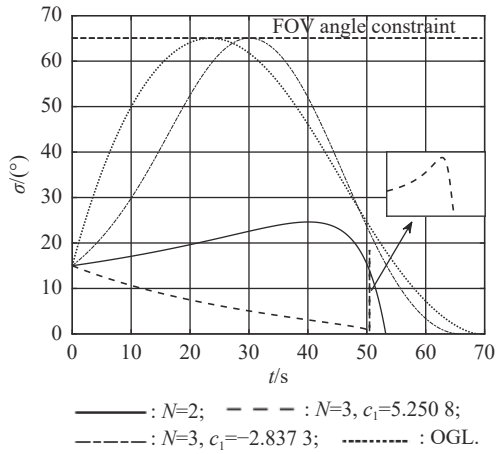

Fig. 15 Looking angle profiles with respect to time

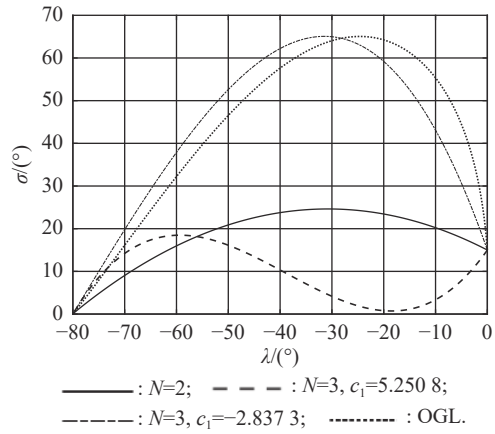

Fig. 16 Looking angle profiles with respect to LOS angle

Since the independent variable of the designed polynomial guidance law is the LOS angle, variations have been redrawn with respect to the LOS angle. Fig. 16 shows that for the third-order shaping guidance law, the looking angle profile for the case of $N = 3(c_1 = 5.250\ 8)$ reaches the maximum and minimum values which are designed previously. The control range of the looking angle for the

third-order shaping guidance law is obviously larger than that of the second-order shaping guidance law. Fig. 17 shows that in the extreme case, the second-order shaping guidance law may not realize the convergence of the terminal lateral acceleration. As shown in Fig. 17 and Fig. 18, the third-order shaping guidance law can realize the convergence of the terminal lateral acceleration within the boundary. However, the maximum lateral acceleration at the end is too large, which needs to be limited in the engineering application.

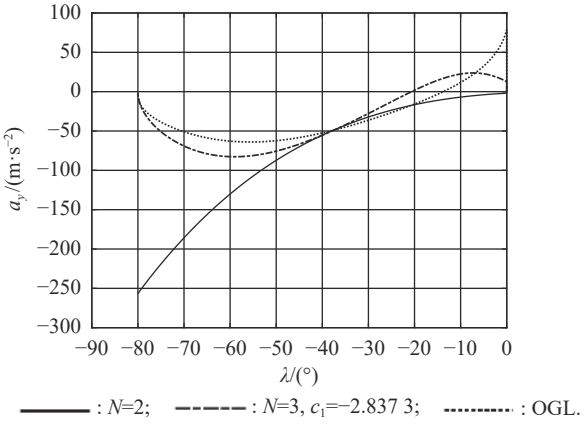

Fig. 17 Lateral acceleration profiles with respect to LOS angle 1

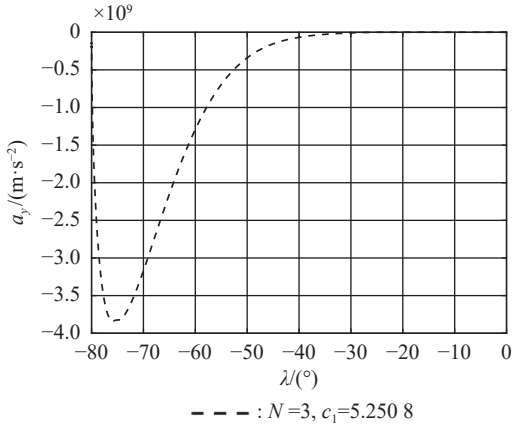

Fig. 18 Lateral acceleration profiles with respect to LOS angle 2

Compared with the traditional OGL, the FOV angle constraint is introduced for the third-order shaping guidance law. In addition, the traditional OGL needs the missile-target relative range to obtain the time-to-go. The shaping guidance law does not need the distance information of the missile and the target. Compared with the second-order shaping guidance law, the proposed guidance law can realize the convergence of the terminal lateral acceleration within the guidance coefficient boundary.

5.3 Realistic simulations

In this section, simulations are carried out with a realistic missile model. Assuming flat, non-rotating Earth, equations of motion can be expressed as

$$\begin{cases} \dfrac{\mathrm{d}x}{\mathrm{d}t} = V\cos\gamma \\ \dfrac{\mathrm{d}y}{\mathrm{d}t} = V\sin\gamma \\ V = \dfrac{T-D}{m} - g \\ \dfrac{\mathrm{d}\gamma}{\mathrm{d}t} = \dfrac{a - g\cos\gamma}{V} \end{cases} \tag{42}$$

where x is the downrange of the missile; y is the altitude; T is the thrust; D is the drag; m is the mass of the missile; g is the gravity acceleration. These parameters are borrowed from [30]. To compensate the gravity acceleration, the guidance law in (16) is augmented as

$$a = \left[c_1(\lambda-\lambda_f)\left(\lambda-\frac{1}{3}\lambda_f\right) + \frac{2(M_f - 1 + \sigma_0/\lambda_f)}{\lambda_f}(\lambda-\lambda_f) + M_f\right]\cdot V\frac{\mathrm{d}\lambda}{\mathrm{d}t} + g\cos\gamma. \tag{43}$$

This case considers different impact angles $\gamma_f = [-60°, -70°, -80°, -90°]$ with FOV angle constraints as $\sigma_{\max} = [30°, 45°, 60°, 75°]$. The terminal guidance law coefficient is designed as $M_f = 3$. Besides, we design the coefficient c_1 as the lower boundary to get the maximum looking angle.

Fig. 19 shows that the missile intercepts the target with different desired impact angles and FOV angle constraints. Fig. 20 shows that the desired impact angles can be satisfied by the proposed guidance law. Looking angles reach the maximum FOV angle and converge to zero at the end as shown in Fig. 21. The lateral acceleration profiles are shown in Fig. 22. Terminal lateral acceleration is convergent, but do not converge to zero due to the compensation of the gravity acceleration in (43). The missile speed profiles decided by aerodynamics are shown in Fig. 23.

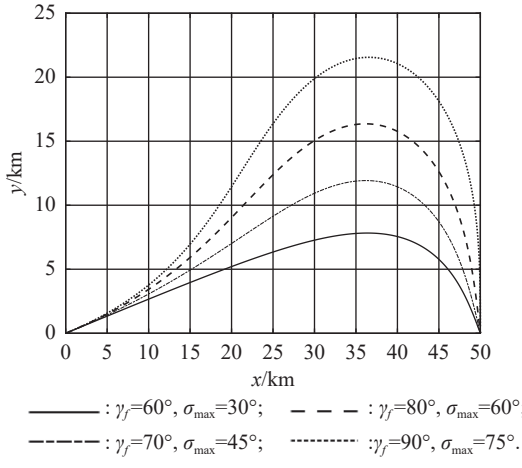

Fig. 19 Missile trajectories with respect to time

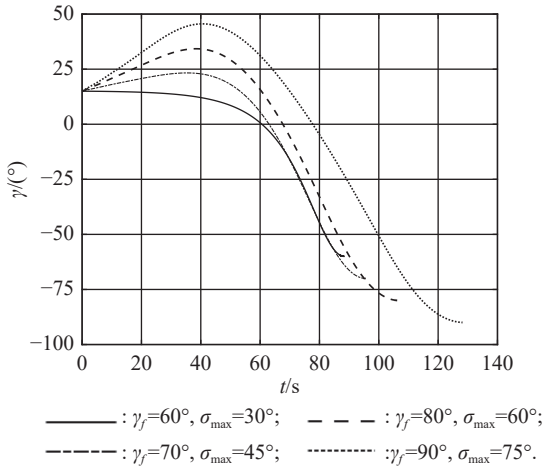

Fig. 20 Flight path angle profiles with respect to time

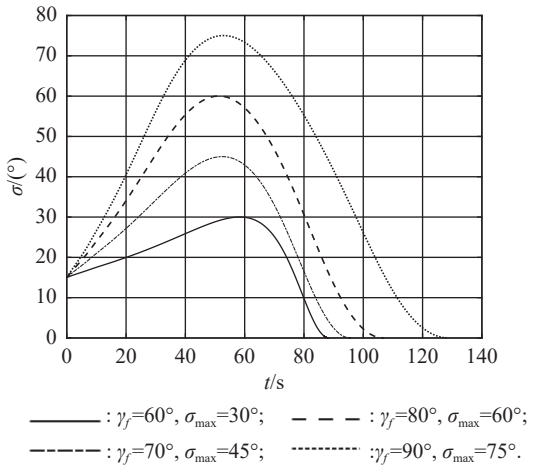

Fig. 21 Looking angle profiles with respect to time

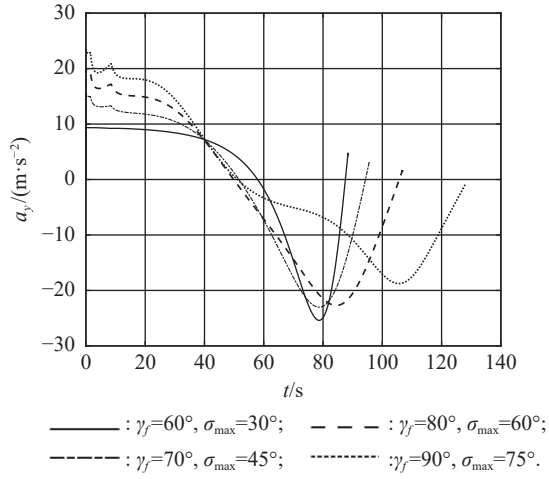

Fig. 22 Lateral acceleration profiles with respect to time

6. Conclusions

To solve the problem that the second-order polynomial shaping guidance law may not satisfy the convergence requirement of the terminal lateral acceleration, we propose a third-order polynomial shaping guidance law. Besides, we analyze the characteristics of the looking angle, which provides adjustment references for the guidance coefficients.

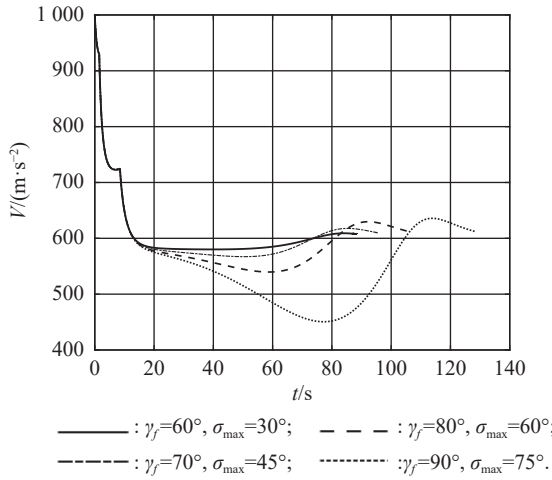

Fig. 23 Speed profiles with respect to time

We transform the range of looking angles into the range of the guidance coefficients, which can satisfy the FOV angle and terminal lateral acceleration constraints simultaneously.

The simulation results show that the third-order polynomial shaping guidance law can satisfy the convergence of the terminal lateral acceleration and the FOV angle constraint, compared with the traditional OGL and the second-order shaping guidance law. Since the proposed guidance law does not need the missile-target relative range, it has a wider application prospect in practice.

References

[1] WANG C Y, DONG W, WANG J N, et al. Nonlinear suboptimal guidance law with impact angle constraint: an SDRE-based approach. IEEE Trans. on Aerospace and Electronic Systems, 2020, 56(6): 4831–4840.

[2] HU Q L, HAN T, XIN M. Three-dimensional guidance for various target motions with terminal angle constraints using twisting control. IEEE Trans. on Industrial Electronics, 2020, 67(2): 1242–1253.

[3] XIN H B, CHEN Q Y, WANG Y J, et al. Terminal guidance simulation and flight test for small UCAV. Proc. of the International Conference on Control, Automation and Diagnosis, 2019: 1431–1441.

[4] KIM H G, LEE J Y, KIM H J. Look angle constrained impact angle control guidance law for homing missiles with bearings-only measurements. IEEE Trans. on Aerospace and Electronic Systems, 2018, 54(6): 3096–3107.

[5] LEE S, KIM Y. Capturability of impact-angle control composite guidance law considering field-of-view limit. IEEE Trans. on Aerospace and Electronic Systems, 2020, 56(2): 1077–1093.

[6] DONG W, WEN Q Q, XIA Q L, et al. Multiple-constraint

cooperative guidance based on two-stage sequential convex programming. Chinese Journal of Aeronautics, 2020, 33(1): 296–307.
[7] KIM M, GRIDER K V. Terminal guidance for impact attitude angle constrained flight trajectories. IEEE Trans. on Aerospace and Electronic Systems, 1973, 9(6): 852–859.
[8] RYOO C K, CHO H, TAHK M J. Closed-form solutions of optimal guidance with terminal impact angle constraint. Proc. of the IEEE Conference on Control Applications, 2003: 504–509.
[9] RYOO C K, CHO H, TAHK M J. Time-to-go weighted optimal guidance with impact angle constraints. IEEE Trans. on Control Systems Technology, 2006, 14(3): 483–492.
[10] KIM K S, JUNG B, KIM Y. Practical guidance law controlling impact angle. Proc. of the Institution of Mechanical Engineers, Part G: Journal of Aerospace Engineering, 2007, 221(1): 29–36.
[11] KUMAR S R, RAO S, GHOSE D. Sliding-mode guidance and control for all-aspect interceptors with terminal angle constraints. Journal of Guidance, Control and Dynamics, 2012, 35(4): 1230–1246.
[12] OZA H, PADHI R. A nonlinear suboptimal guidance law with 3d impact angle constraints for ground targets. Proc. of the AIAA Guidance, Navigation, and Control Conference, 2015: 1–22. DOI: 10.2514/6.2010-8185.
[13] ZARCHAN P. Tactical and strategic missile guidance. Reston: American Institute of Aeronautics and Astronautics, 2012.
[14] LU P, DOMAN D B, SCHIERMAN J D. Adaptive terminal guidance for hypervelocity impact in specified direction. Journal of Guidance, Control and Dynamics, 2006, 29(2): 269–278.
[15] RATNOO A, GHOSE D. Impact angle constrained interception of stationary targets. Journal of Guidance, Control and Dynamics, 2012, 31(6): 1816–1821.
[16] RATNOO A, GHOSE D. Impact angle constrained interception of non-stationary non-maneuvering targets. Journal of Guidance, Control and Dynamics, 2010, 33(1): 269–275.
[17] ERER K S, MERTTOPCUOGLU O. Indirect impact-angle-control against stationary targets using biased pure proportional navigation. Journal of Guidance, Control and Dynamics, 2012, 35(2): 700–704.
[18] ZHANG Y N, MA G X. Guidance law with impact time and impact angle constraints. Chinese Journal of Aeronautics, 2013, 16(4): 960–966.
[19] ZHANG Y A, MA G X, WU H L. A biased proportional navigation guidance law with large impact angle constraint and the time-to-go estimation. Proc. of the Institution of Mechanical Engineers, Part G: Journal of Aerospace Engineering, 2014, 228(G10): 1725–1734.
[20] KIM T H, PARK B G, TANK M J. Bias-shaping method for biased proportional navigation with terminal-angle constraint. Journal of Guidance, Control and Dynamics, 2013, 36(6): 1810–1816.
[21] ERER K S, TEKIN R, OZGOREN M K. Look angle constrained impact angle control based on proportional navigation. Proc. of the AIAA Guidance, Navigation, and Control Conference, 2013: 1–11. DOI: 10.2514/6.2015-0091.
[22] TEKIN R, ERER K S. Switched-gain guidance for impact angle control under physical constraints. Journal of Guidance, Control and Dynamics, 2015, 38(2): 205–216.
[23] PARK B G, KIM T H, TAHK M J. Optimal impact angle control guidance law considering the seeker's field-of-view limits. Proc. of the Institution of Mechanical Engineers, Part G: Journal of Aerospace Engineering, 2012, 227(8): 1347–1364.
[24] PARK B G, KIM T H, TAHK M J. Range-to-go weighted optimal guidance with impact angle constraint and seeker's look angle limits. IEEE Trans. on Aerospace and Electronic Systems, 2016, 52(3): 1241–1256.
[25] RATNOO A. Analysis of two-stage proportional navigation with heading constraints. Journal of Guidance, Control and Dynamics, 2015, 39(1): 1–9.
[26] JEON I S, LEE J I. Impact-time-control guidance law with constraints on seeker look angle. IEEE Trans. on Aerospace and Electronic Systems, 2017, 53(5): 2621–2627.
[27] LIU B J, HOU M S, FENG D. Nonlinear mapping based impact angle control guidance with seeker's field-of-view constraint. Aerospace Science and Technology, 2019, 86(3): 724–736.
[28] SHARMA Y R, RATNOO A. A bearings-only trajectory shaping guidance law with look-angle constraint. IEEE Trans. on Aerospace and Electronic Systems, 2019, 55(6): 3303–3315.
[29] LI R, XIA Q L, WEN Q Q. Extended optimal guidance law with impact angle and acceleration constriants. Journal of Systems Engineering and Electronics, 2014, 25(5): 868–876.
[30] KEE P E, DONG L, SIONG C J. Near optimal midcourse guidance law for flight vehicle. Proc. of the AIAA Aerospace Sciences Meeting and Exhibit, 1998. DOI: 10.2514/6.1998-583.

Biographies

FU Shengnan was born in 1993. She received her B.E. degree from Beijing Institute of Technology, Beijing, China, in 2014. She is currently a doctoral student in the School of Mechatronical Engineering, Beijing Institute of Technology. Her main research interests include flight vehicle design, guidance and control.
E-mail: 3120160497@bit.edu.cn

ZHOU Guanqun was born in 1992. He received his B.E., M.S. and Ph.D. degrees from the School of Aerospace Engineering, Beijing Institute of Technology, Beijing, China, in 2014, 2017 and 2020, respectively. He is currently working in Beijing Aerospace Technology Institute. His research interests include trajectory optimization, design of guidance laws and tracking controllers.
E-mail: zhougq5307@163.com

XIA Qunli was born in 1971. He received his B.E. degree in launcher and design from Beijing Institute of Technology in 1993, and M.S. degree in flight mechanics from Beijing Institute of Technology in 1996. He received his Ph.D. degree in aircraft design from Beijing Institute of Technology in 1999. He is an adjunct professor in Beijing Institute of Technology. His research interests are control and guidance technology.
E-mail: 1010@bit.edu.cn